Journal of Electroanalytical Chemistry 668 (2012) 119–125

Contents lists available at SciVerse ScienceDirect

Journal of Electroanalytical Chemistry

journal homepage: www.elsevier.com/locate/jelechem

Carrier density and interfacial kinetics of mesoporous TiO_2 in aqueous electrolyte determined by impedance spectroscopy

Sixto Gimenez *, Halina K. Dunn, Pau Rodenas, Francisco Fabregat-Santiago, Sara G. Miralles, Eva M. Barea, Roberto Trevisan, Antonio Guerrero, Juan Bisquert *

Photovoltaics and Optoelectronic Devices Group, Departament de Física, Universitat Jaume I, 12071 Castelló, Spain

ARTICLE INFO

Article history:
Received 12 December 2011
Received in revised form 21 December 2011
Accepted 23 December 2011
Available online 11 January 2012

Keywords:
Water splitting
Titanium oxide
Porous semiconductors
Transmission line
Impedance spectroscopy

ABSTRACT

Water splitting at a semiconductor/solution interface with the only input of sunlight to generate hydrogen is one of the most attractive strategies to produce and store chemical energy. In the present study we have investigated carrier dynamics and interfacial kinetics of mesoporous TiO_2 in an aqueous solution. The applicability of the transmission line model for mesoporous semiconductors has been validated to identify chemical capacitance, transport resistance and charge transfer resistance in this system by testing samples of different thicknesses in the dark and under illumination. We found that both transport resistance and chemical capacitance scale well with sample thickness, while charge transfer resistance scales with thickness when the FTO substrate is not exposed to the solution. Otherwise, there is a competition between charge transfer through TiO_2 and through the FTO substrate. Under illumination, the electron density is dominated by photogenerated carriers at biases below the open circuit potential, whereas at higher bias, the applied potential determines the electron density. Evidence of charge transfer via surface states has been experimentally observed and corroborated with a physical model, which explicitly includes charge transfer through a monoenergetic trap for electron and holes. This study may lay the basis for understanding more complex processes at anodic potentials on the TiO_2/solution interface where water splitting reactions take place.

1. Introduction

With the increasing global demand for energy, the need to adopt alternative energy sources is concomitantly growing. Among all the different renewable energy sources presently available, solar energy is the only potential candidate to satisfy the global energy needs [1]. Collecting and storing solar energy in chemical bonds, as nature accomplishes through photosynthesis, is an attractive means to solve the energy challenge [2]. One promising strategy to store energy from sunlight is the photo-assisted splitting of water to generate hydrogen, a clean and portable energy carrier, which can be used to supply electricity upon demand [2,3].

Since the seminal report of Fushijima and Honda in 1972 [4], demonstrating the photocatalytic effect of TiO_2 for electrochemical water splitting, intensive efforts have been dedicated to enhance the efficiency of this material by different strategies: (i) extending the absorption range to the visible (C [5], N [6] and S [7] doping) (ii) tuning the energy of the conduction band (CB) to withstand the hydrogen evolution reaction (HER) by alloying with Ba or Sr). Indeed, $SrTiO_3$ has been the only material showing water splitting without external assistance, although with efficiencies lower than 1% [8]. Moreover, the molecular mechanisms for the involved reactions have been thoroughly studied. Particular attention has been given to the four-hole oxygen evolution reaction (OER) on TiO_2 surfaces, since this reaction has been identified as the rate limiting step of the process. Salvador suggested a mechanism for water oxidation based on the formation of $OH^{\cdot}$ radicals on the surface, followed by the formation of H_2O_2, which is finally oxidized to O_2 [9–12]. This type of intermediates could build up at the surface to allow a sufficient number of holes to accumulate in the same place, in line with the suggestion made by Cowan et al. [13] On the other hand, Nakato and co workers [14,15] reported that the OER is not initiated by the electron transfer-type oxidation, but by a nucleophilic attack of an H_2O molecule (Lewis base) to a surface-trapped hole (Lewis acid), accompanied by bond breaking. Consequently, understanding charge carriers dynamics for both electrons and holes is essential for the evaluation of candidate materials and for the identification of relevant mechanisms in the process.

Previous investigations of electrochemical impedance spectroscopy (EIS) employed to elucidate molecular mechanisms at the TiO_2/solution interface highlighted the key role of surface states on the electrode kinetics [16–19]. The present study is aimed at

* Corresponding authors. Tel.: +34 964387554; fax: +34 964729218.
E-mail addresses: sjulia@fca.uji.es (S. Gimenez), bisquert@fca.hji.es (J. Bisquert).

1572-6657/$ - see front matter © 2012 Elsevier B.V. All rights reserved.
doi:10.1016/j.jelechem.2011.12.019

obtaining information about carrier dynamics in *mesoporous* TiO_2 by monitoring the electron dynamics, particularly the electron conductivity, recombination resistance and chemical capacitance from impedance spectroscopy measurements. The description of the mesoporous electrode is different from the planar electrode due to the fact that the internal, reactive surface is distributed along the whole film, so that transport and charge transfer process are intimately coupled. To solve this problem we applied the well-established transmission line model [20,21], which has been successfully used to comprehensively understand electron dynamics in dye sensitized solar cells [22]. Here we aim to identify key carrier processes in the case in which both electrons and holes are generated in the semiconductor by UV illumination.

2. Experimental

2.1. Electrode preparation

TiO_2 nanoparticulated films were deposited by screen printing a commercial colloidal paste (Dyesol 18 NT) on transparent conducting fluorine doped tin oxide (FTO) glass substrates (TEC 15 Pilkington TEC Glass™, sheet resistance ~10 Ω/□). The FTO substrates were previously cleaned with detergent and de-ionised water, followed by sonication in isopropanol. Some FTO substrates were coated with a (~100 nm thick) TiO_2 compact layer by spray pyrolisis of titanium(IV)bis(acetoacetonato)di(isopropanoxylate) [23,24]. The resulting photoelectrodes were sintered at 450 °C, in order to achieve good electrical contact between the nanoparticles. The thickness of the as-prepared TiO_2 films (approximately 2.5 μm, 5 μm and 10 μm) was measured by a profilometer Dektack 6 from Veeco.

2.2. Optical and electrochemical characterization

The transmittance and diffuse reflectance spectra of the photoelectrodes were recorded between 300 and 800 nm by a Cary 500 UV–VIS Varian photospectroscometer. An integrating sphere was used for the diffuse reflectance measurements. The absorbance was calculated as:

$$A = -log(T + R) \quad (1)$$

and the absorptivity (α) was calculated from $A = \alpha l$ where l is the thickness of the electrodes.

Current density voltage (j–V) and electrochemical impedance spectroscopy (EIS) measurements were carried out using a FRA equipped PGSTAT-30 from Autolab. A three-electrode configuration was used, where the FTO/TiO_2 electrode was connected to the working electrode, a Pt wire was connected to the counterelectrode and a Ag/AgCl was used as the reference electrode. A 0.5 M KOH solution prepared with Milli-Q water (pH 13) was used. The electrodes were illuminated using a 35 W Xe lamp, where the light intensity was adjusted with a thermopile to 100 mW/cm^2, with illumination through the FTO substrate. EIS measurements were carried out applying 20 mV AC signal and scanning in a frequency range between 400 kHz and 0.1 Hz, at different applied biases. The correction for voltage drop at the series resistance was carried out to accurately determine the potential at the TiO_2 nanostructure (V_F). However, since the measured currents were low (below 0.3 mA/cm^2), this correction did not have any significant influence and it is omitted below.

3. Physical model

In order to establish the theoretical basis of our approach, the employed physical model is described below. Fig. 1a shows a simple scheme of the TiO_2 mesoporous film on top of a conductive FTO substrate. The kinetic processes taking place in the semiconductor and at the semiconductor/liquid interface are summarized in Fig. 1b: upon optical excitation, electron–hole pairs are created in the semiconductor. In water splitting conditions, electrons are transported within the conduction band to the external contact and holes are transferred to the solution to oxidize water. If surface traps are present at the semiconductor/solution interface, both electrons and holes can be captured by this surface state, where they can recombine or be transferred to the solution. The transport of the majority carriers (electrons) takes place at a continuous electron transport level with the corresponding Fermi level (E_{Fn}), while hole transport is not continuous due to their inherent low mobility in the material, as indicated in Fig. 1c.

Fig. 2a represents the general transmission line equivalent circuit, that has been widely used in the analysis of dye-sensitized solar cells [22]. This representation takes into account electron transport (r_{tr}), along the electron transport level, as previously suggested in Fig. 1. The transversal element ζ_m in Fig. 2a depends on charge accumulation and charge transfer, and the lower, resistanceless rail indicates fast transport in the electrolyte. Now considering the water splitting system, we take into account the presence of both electrons and holes in the semiconductor material, which is a situation absent in DSC. Therefore a more complex model is required, and since specific circuits to account for this situation have not yet been developed, to our knowledge, we suggest the circuit of Fig. 2b that has been previously developed for the presence of electrons and holes in related systems [25,26]. This equivalent circuit, that constitutes the element ζ_m in Fig. 2a, is composed of separate chemical capacitances of electrons and holes ($C_\mu^{(cb)}, C_\mu^{(vb)}$) and charge transfer to the solution through the conduction and valence bands ($r_{ct}^{(cb)}$ *and* $r_{ct}^{(vb)}$) together with electron and hole trapping ($r_{trn}^{(ss)}, r_{trp}^{(ss)}, C_\mu^{(ss)}$) and charge transfer ($r_{ct}^{(ss)}$) through

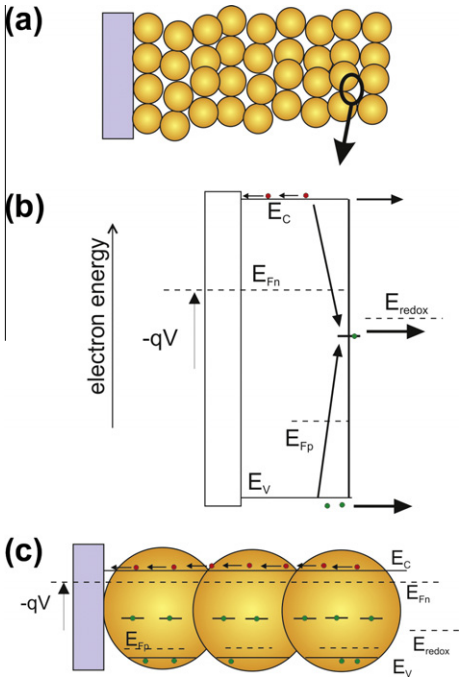

Fig. 1. (a) Scheme of the TiO_2 mesoporous film on the FTO conductive substrate. (b) Kinetic model illustrating the different possible processes in the semiconductor (electron transport to substrate and hole transference to the surface) and at the semiconductor/solution interface (electron and hole trapping at a surface state, charge transfer to the solution through the semiconductor bands and through the surface state). (c) In TiO_2, the transport of the majority carriers (electrons) takes place at a continuous transport level (E_c), while photogenerated holes do not effect long range transport and remain localized close to the generation place.

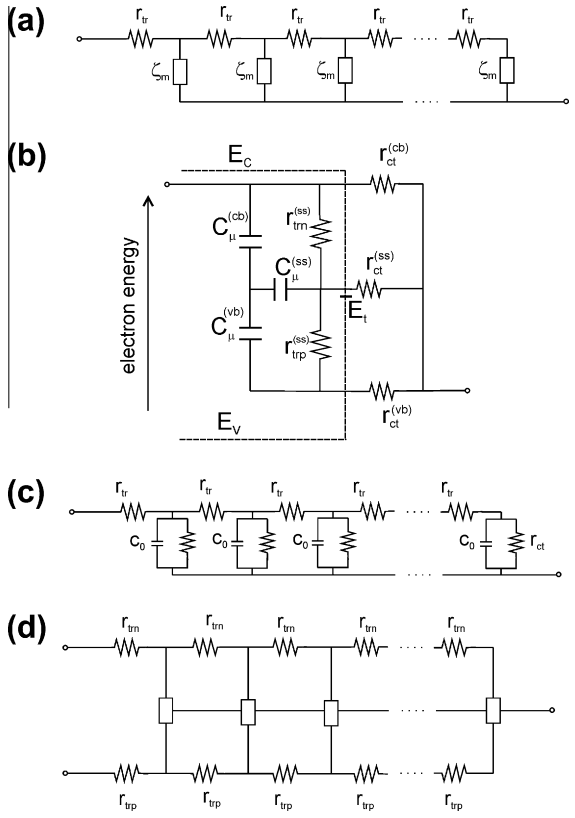

Fig. 2. (a) Two channel transmission line equivalent circuit, with electron transport resistance and the transversal element ζ_m corresponds to the equivalent circuit represented in (b). The meaning of the different elements is indicated in the main text. (c) Simplified equivalent circuit used in the present study including transport, chemical capacitance and charge transfer of electrons. (d) Equivalent circuit including electron and hole transport and the central electrolyte rail. The box does not represent an impedance element but indicates a more complex connection, depending on the kinetic processes of electrons and holes.

the surface state. A simplified equivalent circuit only accounting for the transport, chemical capacitance and charge transfer of electrons is represented in Fig. 2c. This is the equivalent circuit that we used in the present study. If the system shows facile hole transport in the valence band, the model should be extended with a channel for hole transport, included in the equivalent circuit, as indicated in Fig. 2d. Now the model shows the upper rails for electron transport, the lower one for hole transport, and the central one for electrolyte. In Fig. 2d the box does not represent an impedance element but indicates a more complex connection, depending on the specific charge storage, recombination, surface states features, and other specific properties that link electrons, holes and their charge transfer to the solution. But we can see that a cathodic voltage activates electron transport (as discussed in this paper) while anodic potential facilitates hole transport if this is possible in the system. The switch between these two mechanism and the three channel transmission line has been previously demonstrated [27].

4. Results and discussion

The optical absorbance of representative TiO_2 mesoporous films (anatase) of different thicknesses is shown in Fig. 3. The optical bandgap of the material could be estimated by the Tauc plots for indirect bandgap transitions. The obtained value was $E_g = 3.26$ eV in good correspondence with the theoretical value for anatase, $E_g = 3.23$ eV [28,29].

Fig. 4 shows the j–V curves of the mesoporous TiO_2 samples with different thicknesses in the dark and under illumination.

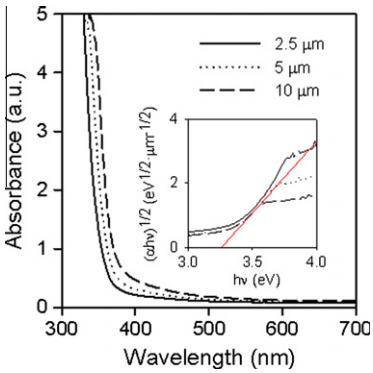

Fig. 3. Absorbance of the TiO_2 films with different thicknesses. Inset: Tauc plot for the estimation of the indirect bandgap transition of the tested TiO_2 samples ($E_g = 3.26$ eV).

The response of the FTO substrate is also included as a reference. The standard equilibrium potentials for the oxygen evolution reaction (OER) and HER at pH 13 (−0.97 V and 0.26 V vs. Ag/AgCl respectively) are also indicated. The dark j–V curves are characterized by a large potential range (1.1 V), where current does not flow through the electrochemical cell. A cathodic current is observed with an onset at −0.5 V vs. Ag/AgCl, which is 0.4 V more positive than the equilibrium potential for HER (−0.97 V vs. Ag/AgCl). At this potential, O_2 reduction to OH^- takes place. At −0.95 V vs. Ag/AgCl a clear cathodic peak is observed related to electron transfer through a localized interbandgap TiO_2 state. The presence of this peak is consistent with observations of trap states made by other researchers [30,31]. However, there is some debate about its physical origin, which has been ascribed either to surface states [32] or to traps at grain boundaries [30]. At positive potentials higher than 0.6 V vs. Ag/AgCl, an exponentially increasing positive current with potential is related to the oxygen evolution reaction through the FTO, which has a valence band edge position 0.7 V more positive compared to anatase TiO_2 [1]. Under illumination, a positive photocurrent is observed due to photogenerated holes. This photocurrent does not scale linearly with the sample thickness. Additionally, the cathodic peak associated to electron transfer through surface states in TiO_2 is less pronounced and in some cases disappears completely. This behavior could be explained by the presence of photogenerated holes, which recombine with electrons located at surface states, this process being faster than charge transfer to the solution.

As previously discussed, our aim is to obtain information about electrons and holes dynamics in TiO_2 by monitoring the electron conductivity, recombination resistance and chemical capacitance via impedance spectroscopy measurements. In order to validate the applicability of the transmission line model of Fig. 2c to the study of porous TiO_2 in an aqueous electrolyte, the effect of the film thickness was studied at forward bias. If the film is uniformly porous and charge transfer can occur throughout the whole internal surface area, we expect the capacitance and transport resistance to scale linearly with film thickness, and the charge transfer resistance to scale inversely with thickness.

Fig. 5 shows the EIS spectra at −0.95 V Ag/AgCl for TiO_2 samples with three different thicknesses in the dark and under illumination. At this potential, the measured spectra are characterized by an arc closing at low frequencies, related to chemical capacitance (C_μ) and charge transfer resistance (R_{ct}), and a 45° line observed at high frequencies (Fig. 5b) which is related to electron diffusion through the mesoporous film [20,33]. The length of this line corresponds to one third of the transport resistance, $R_t/3$. The transport resistance (per unit macroscopic area, cm^{-2}) relates to the electron conductivity, σ_n and film thickness, L, as

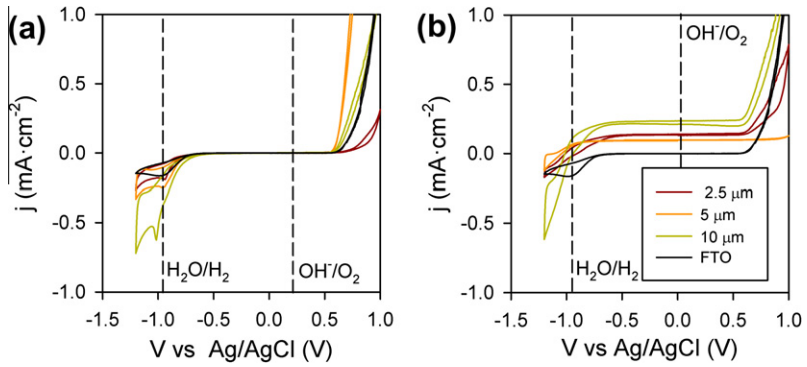

Fig. 4. *j–V* curves of samples of mesoporous TiO_2 with different thicknesses in the dark (a) and under illumination (b). The *j–V* curve of the FTO substrate is also showed as a reference.

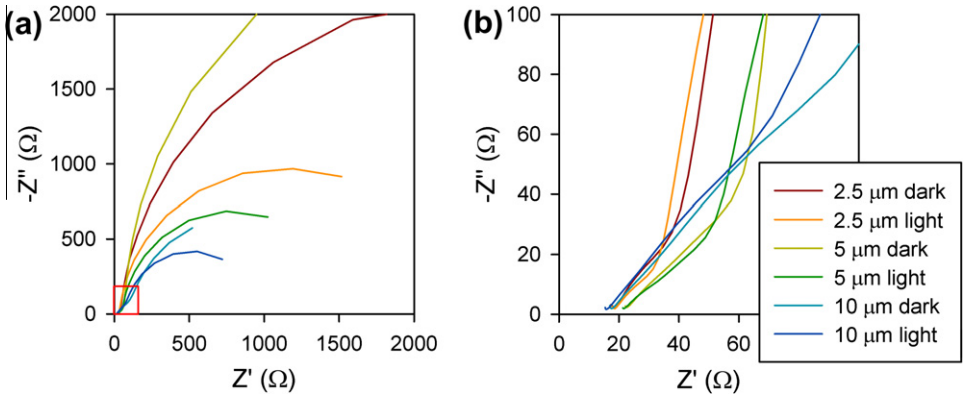

Fig. 5. (a) EIS spectra obtained at −0.95 V vs. Ag/AgCl in the dark and under illumination at 100 mW cm^{-2}. (b) Magnification of the squared area in (a) to illustrate the 45° line related to transport resistance.

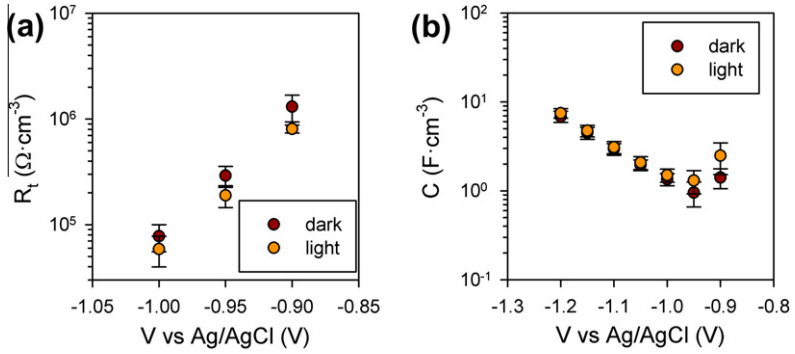

Fig. 6. Volumetric transport resistance (a) and volumetric capacitance (b) of three thicknesses of porous TiO_2 as a function of potential in the dark and under illumination.

$$R_t = \frac{L}{\sigma_n} \tag{2}$$

From Fig. 5b it is clear that the thicker the TiO_2 film, the higher the transport resistance of the material in good agreement with Eq. (2). Additionally, illuminated samples show a slightly lower transport resistance.

The quantitative correlation between volumetric conductivity and capacitance with film thickness is illustrated in Fig. 6. A minimum of two samples of each thickness (2.5 μm, 5 μm and 10 μm) were characterized for each point in this figure. The error bars indicate the scatter between the different samples. It is clear that the transport resistance, Fig. 6a, scales linearly with sample thickness both in the dark and under illumination.

Similarly, C_μ scales linearly with the thickness both in the dark and under illumination (Fig. 6b). Again, here we show the average volumetric capacitance for at least two samples of each thickness. Since the chemical capacitance is determined by the Fermi level of the electrons, which is governed by the external bias, no significant difference between dark and illumination was obtained over most of the voltage range. However, at potentials more positive than −1V vs Ag/AgCl (Fig. 6b), the capacitance is higher, and the transport resistance lower, under illumination.

Fig. 7 shows the capacitance and charge transfer resistance for TiO_2/FTO films with different thicknesses of TiO_2, together with blank samples (only FTO). At potentials more positive than −0.9 V vs. Ag/AgCl, both C_μ and R_{ct} are dominated by the FTO

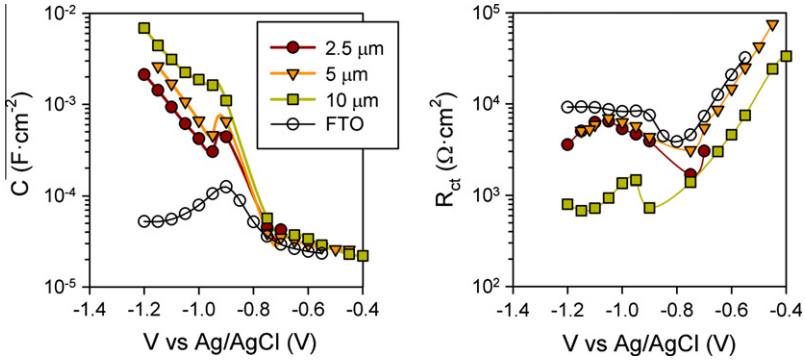

Fig. 7. Charge transfer resistance and chemical capacitance of a 10 μm (squares), 5 μm (triangles), 2.5 μm (filled circles) TiO_2 film deposited on a FTO substrate in the dark. Also shown are R_{ct} and C_μ of a bare FTO substrate (empty circles). The lines are plotted as a guide for the eye.

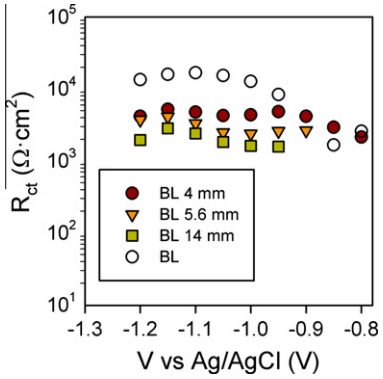

Fig. 8. Charge transfer resistance of films of various thicknesses (4, 5.6 and 14 μm) in the presence of a compact blocking layer (BL) under illumination. The results for a reference sample without mesoporous TiO_2 (BL) is also included for comparison.

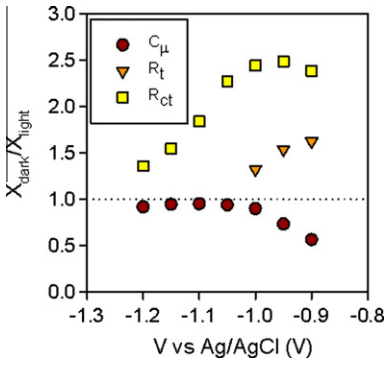

Fig. 9. Effect of illumination on the chemical capacitance, charge transfer and transport resistances of TiO_2 films deposited directly on FTO substrates. *X* refers to either chemical capacitance (C_μ), transport resistance (R_t) or charge transfer resistance (R_{ct}).

substrate, while at values more negative than than −0.9 V vs. Ag/AgCl, C_μ becomes clearly dominated by the TiO_2 film. This corresponds to the potential at which R_t becomes visible, indicating the transition between insulating and conducting TiO_2. The trend in charge transfer resistance, on the other hand, is less clear. The two thinner films essentially behave the same as the FTO substrate alone. The 10 μm film has a lower R_{ct}, as expected due to the larger surface area, but also a different shape, which is more closely related to that of the capacitance (capacitance peak coincident with a valley in the charge transfer resistance). This characteristic capacitance - charge transfer correspondence at V = −0.8 V vs. Ag/AgCl is likely to be due to charge transfer via a surface state, as discussed below [34].

The observation that charge transfer resistance does not scale with thickness is explained by considering charge transfer through the FTO substrate as a competing pathway. Consequently, only when a certain TiO_2 film thickness is reached, charge transfer takes place through TiO_2. If the FTO substrate is passivated by growing a 100 nm TiO_2 compact layer between FTO and the mesoporous TiO_2, R_{ct} scales qualitatively well with thickness as shown in Fig. 8.

4.1. Effect of illumination

The results obtained for R_t, C_μ, and R_{ct} confirm that the transmission line model describes the behaviour of TiO_2 electrodes satisfactorily. Upon UV illumination, electrons are excited to the conduction band of TiO_2, leaving holes in the valence band. It can therefore be informative to consider the difference in the average volumetric parameters between dark and illuminated conditions. In Fig. 9 we present the ratio of the average volumetric R_{ct}, C_μ and R_t values in the dark and under illumination (indicated as X_{dark}/X_{light}) as a function of the applied potential. These averages are calculated from at least two samples of each thickness (2.5, 5 and 10 μm).

Between −0.9 and −1 V vs. Ag/AgCl, C_μ is higher under illumination, before converging to the dark values. R_t is also lower under illumination. These observations indicate that under illumination at a given potential between −0.9 and −1 V, there are more electrons present, with respect to the dark situation. This voltage range coincides with the cathodic voltammetry peak, which is associated with a surface state. However, although C_μ may encompass both bulk and surface states, it is unlikely that R_t would be influenced by surface states. We further note that the open circuit potential of the cell under illumination is around −1 V vs. Ag/AgCl. This observation reflects the fact that below the open circuit potential, the applied potential lies below the Fermi level of photogenerated carriers.

Hence the two parameters most sensitive to the bulk of the material agree on the presence of excess electrons under illumination. In contrast, R_{ct}, which is sensitive only to surface processes, exhibits a much stronger dependence on illumination, which persists well above −1 V. The presence of photogenerated holes, which can recombine with electrons reduces R_{ct}. Additionally, the local increase of temperature upon illumination may also enhance the charge transfer kinetics.

4.2. Charge transfer through a localized surface state

Porous TiO_2 is expected to have an exponential distribution of interbandgap states, which ought to be translated as an exponential increase in C_μ, along with a corresponding decrease

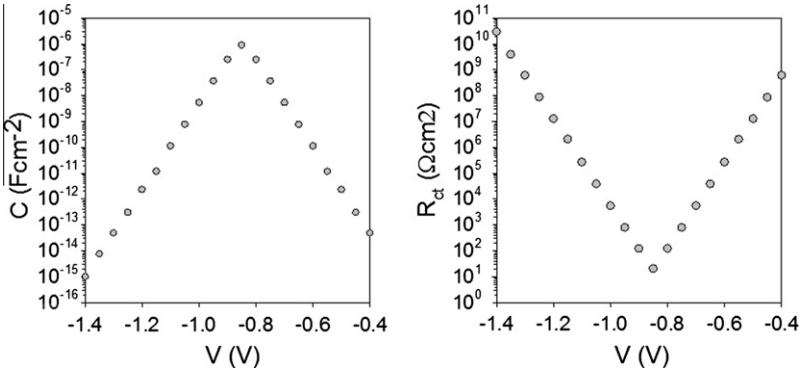

Fig. 10. Model simulation of C_μ and R_{ct} of the surface state as a function of applied voltage.

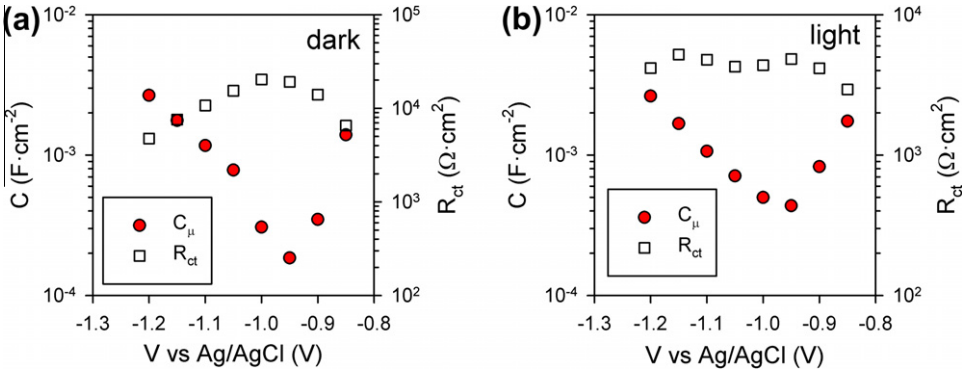

Fig. 11. C_μ and R_{ct} of a 4 μm film deposited on a compact blocking layer in the dark (a) and under illumination (b).

in R_{ct}. Energetically localised surface states are expected to lead to a peak in capacitance along with a dip in charge transfer resistance [34,35].

In order to describe this behavior, we have developed a general model of trapping and charge transfer, assuming that surface states are concentrated at a monoenergetic level. Illumination promotes electrons from the valence band to the conduction band, creating holes in the valence band. These holes might be trapped in the surface state or transferred to the solution. Electrons can be extracted or might recombine at the trap level. Electron transfer to the solution occurs via the surface state. By applying a small perturbation to the conservation equations in the frequency domain, impedance is calculated [17]. Fig. 10 shows the simulated charge transfer resistance and chemical capacitance of the surface state. Both have been calculated through the simulated impedance at different voltage steps, obtained from the model described before. The charge transfer resistance exhibits an exponential decay until the trap level is reached, followed by an exponential increase. In accordance with this fact, chemical capacitance presents a maximum at the same voltage and an exponential increase (decrease) before (after) the energy trap level.

An identical behaviour has been experimentally observed as shown in Fig. 7 and more clearly in Fig. 11, where the dependence of both R_{ct} and C_μ on applied potential for cells built on a compact blocking layer is illustrated. At −0.85 V, there is a sharp decrease in C_μ, and a corresponding increase in R_{ct} in perfect agreement with the results of the model. The whole capacitance peak is not observed, as at potentials more positive than −0.8 V the impedance spectrum is dominated by the FTO substrate, given that this is the potential at which we begin to observe transport. At potentials more negative than −0.95 V there is an exponential increase in C_μ, and a corresponding decrease in R_{ct}. Under illumination, R_{ct} is almost independent of voltage, indicating that charge transfer is affected by the photogenerated holes.

5. Summary and conclusions

We have carried out a systematic study to investigate the carrier density and interfacial kinetics of mesoporous TiO_2 by impedance spectroscopy. We used TiO_2 films with different thicknesses in order to validate the transmission line model under forward bias. The perfect scaling of chemical capacitance and transport resistance with film thickness both in the dark and under illumination validates the applicability of the model. The limited correlation of charge transfer resistance with film thickness could be explained by the preferential charge transfer through FTO until a certain thickness is reached. When charge transfer through FTO was inhibited, a good qualitative correlation between R_{ct} and film thickness has been obtained. A characteristic footprint for the presence of surface states is observed for the j–V curves, capacitance (and under certain conditions also for charge transfer resistance), in good correlation with the developed model, which considers electron and hole transfer through a surface state. C_μ, R_t or R_{ct} are all controlled by illumination at potentials more positive than the open circuit potential of the cell (around −1 V vs. Ag/AgCl). At more negative applied potentials, C_μ and R_t are defined by the electron Fermi level, whereas R_{ct} is affected by the presence of photogenerated holes. This study may lay the basis for understanding more complex processes at anodic potentials on the TiO_2/solution interface where water splitting reactions take place.

Acknowledgements

The authors acknowledge the support of from Ministerio de Cíencia e Innovación under Project HOPE CSD2007-00007 and the Ramon y Cajal program and Generalitat Valenciana under Project PROMETEO/2009/058.

References

[1] R. van de Krol, Y.Q. Liang, J. Schoonman, Journal of Materials Chemistry 18/20 (2008) 2311.
[2] K. Maeda, K. Domen, Journal of Physical Chemistry Letters 1/18 (2010) 2655.
[3] J. Bisquert, Journal of Physical Chemistry Letters 2/3 (2011) 270.
[4] A. Fujishima, K. Honda, Nature 238/5358 (1972) 37.
[5] S.U.M. Khan, M. Al-Shahry, W.B. Ingler, Science 297/5590 (2002) 2243.
[6] R. Asahi, T. Morikawa, T. Ohwaki, K. Aoki, Y. Taga, Science 293/5528 (2001) 269.
[7] T. Umebayashi, T. Yamaki, H. Itoh, K. Asai, Applied Physics Letters 81/3 (2002) 454.
[8] J.G. Mavroides, J.A. Kafalas, D.F. Kolesar, Applied Physics Letters 28/5 (1976) 241.
[9] C. Gutierrez, P. Salvador, Journal of the Electrochemical Society 133/5 (1986) 924.
[10] P. Salvador, Journal of Physical Chemistry 89/18 (1985) 3863.
[11] P. Salvador, F. Decker, Journal of Physical Chemistry 88/25 (1984) 6116.
[12] P. Salvador, C. Gutierrez, Surface Science 124/2–3 (1983) 398.
[13] A.J. Cowan, J.W. Tang, W.H. Leng, J.R. Durrant, D.R. Klug, Journal of Physical Chemistry C 114/9 (2010) 4208.
[14] A. Imanishi, T. Okamura, N. Ohashi, R. Nakamura, Y. Nakato, Journal of the American Chemical Society 129/37 (2007) 11569.
[15] R. Nakamura, T. Okamura, N. Ohashi, A. Imanishi, Y. Nakato, Journal of the American Chemical Society 127/37 (2005) 12975.
[16] D. Vanmaekelbergh, F. Cardon, Journal of Physics D–Applied Physics 19/4 (1986) 643.
[17] E.A. Ponomarev, L.M. Peter, Journal of Electroanalytical Chemistry 397/1–2 (1995) 45.
[18] Z. Hens, Journal of Physical Chemistry B 103/1 (1999) 122.
[19] W.H. Leng, Z. Zhang, J.Q. Zhang, C.N. Cao, Journal of Physical Chemistry B 109/31 (2005) 15008.
[20] J. Bisquert, Journal of Physical Chemistry B 106/2 (2002) 325.
[21] J. Bisquert, G. Garcia-Belmonte, F. Fabregat-Santiago, N.S. Ferriols, P. Bogdanoff, E.C. Pereira, Journal of Physical Chemistry B 104/10 (2000) 2287.
[22] F. Fabregat-Santiago, J. Bisquert, G. Garcia-Belmonte, G. Boschloo, A. Hagfeldt, Solar Energy Materials and Solar Cells 87/1–4 (2005) 117.
[23] A. Braga, S. Gimenez, I. Concina, A. Vomiero, I. Mora-Sero, Journal of Physical Chemistry Letters 2/5 (2011) 454.
[24] V. Gonzalez-Pedro, X.Q. Xu, I. Mora-Sero, J. Bisquert, Acs Nano 4/10 (2010) 5783.
[25] P.C.H. Chan, C.T. Sah, Ieee Transactions on Electron Devices 26/6 (1979) 924.
[26] I. Mora-Sero, Y. Luo, G. Garcia-Belmonte, J. Bisquert, D. Munoz, C. Voz, J. Puigdollers, R. Alcubilla, Solar Energy Materials and Solar Cells 92/4 (2008) 505.
[27] J. Bisquert, M. Gratzel, Q. Wang, F. Fabregat-Santiago, Journal of Physical Chemistry B 110/23 (2006) 11284.
[28] M.V. Rao, K. Rajeshwar, V.R. Paiverneker, J. Dubow, Journal of Physical Chemistry 84/15 (1980) 1987.
[29] Y.K. Kho, A. Iwase, W.Y. Teoh, L. Madler, A. Kudo, R. Amal, Journal of Physical Chemistry C 114/6 (2010) 2821.
[30] T. Berger, T. Lana-Villarreal, D. Monllor-Satoca, R. Gomez, Journal of Physical Chemistry C 111/27 (2007) 9936.
[31] H.L. Wang, J.J. He, G. Boschloo, H. Lindstrom, A. Hagfeldt, S.E. Lindquist, Journal of Physical Chemistry B 105/13 (2001) 2529.
[32] N. Kopidakis, N.R. Neale, K. Zhu, J. van de Lagemaat, A.J. Frank, Applied Physics Letters 87/20 (2005).
[33] J. Bisquert, F. Fabregat-Santiago (Eds.), Dye-sensitized Solar Cells, CRC Press, Boca Ratón, 2010.
[34] I. Mora-Sero, J. Bisquert, Nano Letters 3/7 (2003) 945.
[35] J. Bisquert, Journal of Electroanalytical Chemistry 646 (2010) 43.